

## Quantum Thermodynamics: Non-equilibrium 3D Description of an Unbounded System at an Atomistic Level

A. Sciacovelli<sup>2\*</sup>, C. E. Smith<sup>1</sup>, M. R. von Spakovsky<sup>1\*\*</sup>, and V. Verda<sup>2</sup>

<sup>1</sup>Center for Energy Systems Research, Mechanical Engineering Department  
Virginia Polytechnic Institute and State University, Blacksburg, VA 24061, U.S.A.

<sup>2</sup>Department of Energy Engineering  
Politecnico di Torino, c.so Duca degli Abruzzi 24, 10129 Torino, ITALY

E-mail: adriano.sciacovelli@polito.it, cesmith@vt.edu, michael.von.spakovsky@vt.edu, vittorio.verda@polito.it

### Abstract

Quantum thermodynamics (QT) provides a general framework for the description of non-equilibrium phenomena at any level, particularly the atomistic one. This theory and its dynamical postulate are used here to extend the work reported in previous papers of modeling the storage of hydrogen in an isolated system, by extending the modeling to 3D. The system is prepared in a state with the hydrogen molecules initially far from stable equilibrium after which the system is allowed to relax (evolve) to a state of stable equilibrium. The so-called energy eigenvalue problem, which entails a many-body problem that for dilute and moderately dense gases can be solved using virial expansion theory, is used to determine the energy eigenvalues and eigenstates of the system. This information is then used in the nonlinear Beretta equation of motion of QT to determine the evolution of the thermodynamic state of the system as well as the spatial distributions of the hydrogen molecules in time. The results of our simulations provide a quantification of the entropy generated due to irreversibilities at an atomistic level and show in detail the trajectory of the state of the system as the hydrogen molecules, which are initially arranged to be far from the carbon nanotube, spread out in the system and eventually become more concentrated near the carbon atoms which make up the nanotube

**Keywords:** *Quantum thermodynamics, non-equilibrium, entropy generation, nanoscale systems, atomistic modeling.*

### 1. Introduction

Existing theories of physical reality, namely, mechanics (quantum and classical) and equilibrium thermodynamics, give rise to a number of disciplines including quantum chemistry - QC, density functional theory - DFT, statistical thermodynamics - ST, statistical quantum mechanics - SQM, statistical classical mechanics - SCM (e.g., the kinetic theory of gases), and molecular dynamics - MD. QC, DFT, and ST are used to model the equilibrium characteristics of systems starting from the atomistic level, while SQM, SCM, and MD attempt to describe the non-equilibrium path that a system takes at the atomistic and mesoscopic levels. To determine the equilibrium characteristics, QC, DFT, and ST either apply the minimum energy principle or the maximum entropy principle in a constrained optimization to arrive at the property expressions of equilibrium thermodynamics but are unable to describe the evolution in state which a system undergoes, i.e., the *non-equilibrium* thermodynamic path which the system takes. SQM and SCM provide such a description, predicting the entropy generation via either some quantum master equation (e.g., the Kossakowski-Sudarshan-Gorini-Lindblad (KSGL) equation (Kossakowski, 1972; Ingarden and Kossakowski, 1975; Lindblad, 1976)) or classical master equation (e.g., the BGK and Fokker-Planck equations (Liboff, 1979; Harris, 1999)) but do so at the expense of introducing a paradox, i.e., the so-called Loschmidt paradox. Thus, for example, the KSGL equation

assumes that the entropy generation is due to a rapid erasure of the exogenous statistical correlations between the system and a weakly coupled energy reservoir (Gorini, Kossakowski, and Sudarshan, 1976), which, of course, contradicts the underlying reversible unitary dynamics of the equation itself. Similarly, the entropy generation resulting from the classical master equation is due to assuming a mechanism of loss of correlations between one collision and the next, which is necessary to obtain the classical Boltzmann equation from which the classical master equations are derived, but is incompatible with the assumed underlying reversible Hamiltonian-Liouville dynamics. In both cases, the inevitable conclusion drawn is that the entropy generation due to irreversibility emerges as a kind of *statistical illusion*. The sixth discipline, MD, when coupled with an assumption that the states of a system at least locally pass to some approximation through a series of equilibrium states, is able to provide a pseudo-thermodynamic description of a system's evolution in state but this, of course, is at best incomplete.

There is an alternate theory of physical reality, however, namely, quantum thermodynamics (QT) (Hatsopoulos and Gyftopoulos, 1976a,b,c,d; Beretta, 1981; Beretta et al., 1984) that provides a general framework for the description of non-equilibrium phenomena at any level, particularly the atomistic one. QT avoids the Loschmidt paradox, eschewing the exogenous statistical description for a purely endogenous one and completing the linear dynamics of

\* This paper was published in the ECOS09 proceedings and is printed here with modifications and with permission of the authors and organizers.

\*\* Corresponding author

conventional quantum mechanics with one which is fully non-linear (von Spakovsky, 2008). QT is used here to extend the work reported in previous papers (von Spakovsky, Smith, and Verda, 2008; Smith, Verda, and von Spakovsky, 2008) of modeling the storage of hydrogen in an isolated system, by extending the 1D and 2D modeling to 3D. Thus, the so-called energy eigenvalue problem, which describes the spatial part of the QT description and entails a many-body problem that for dilute and moderately dense gases can be solved using virial expansion theory (e.g., Tien and Lienhard, 1979; Hill, 1956), is solved in 3D to determine the primitive-level energy eigenvalues and eigenstates of the system. This information is then used in a combinatorial problem to determine the system-level energy eigenvalues and eigenstates, which are used in the nonlinear Beretta equation of motion of QT (Beretta, 1981, 2005, 2006a,b, 2007, 2008; Beretta et al., 1984, 1985; Gheorghiu-Svirschevski, 2001) to determine the evolution of the thermodynamic state of the system that initially is prepared in a state with the hydrogen molecules far from stable equilibrium. The spatial distributions of the hydrogen molecules in time are then determined using the solutions found from the spatial and temporal parts of the QT description. The results of our simulations provide a quantification of the entropy generated due to irreversibilities at an atomistic level and show in detail the trajectory of the state of the system as the hydrogen molecules, which are initially arranged to be far from the carbon nanotube, spread out in the system and eventually become more concentrated near the carbon atoms which make up the nanotube.

## 2. Application of QT TO H<sub>2</sub> Storage on Carbon Nanotubes

### 2.1 System Description

The system modeled here is that of 4 H<sub>2</sub> molecules contained in a 5 nm x 5 nm x 10 nm tank with a carbon nanotube at its center. The nanotube is constructed based on Frey and Doren (2005) and is characterized by a (3,3) chiral vector and a chiral angle of 30°. These two parameters define the helical arrangement of the tube. Each tube ring consists of 6 carbon atoms and 22 rings are considered here. The fundamental lattice consists of 6 hexagonal sub-cells. The total number of carbon atoms is 132. The radius and the length of the tube are 0.52 nm and 4.0 nm, respectively. The carbon nanotube is located at the center of the tank so that the center of the tube is placed at coordinate (5,2.5,2.5). Figure 1 presents two schematic views of the tank and the carbon nanotube.

### 2.2 System of Governing Equations

The governing equations for the evolution in time of the thermodynamic state and position of the H<sub>2</sub> molecules are given, respectively, by the system of equations (one equation for each non-zero member  $\rho_i$  of the diagonal state operator or matrix  $\hat{\rho}$ , e.g., see Beretta, 2006b; Smith and von Spakovsky, 2007) represented by the Beretta equation of motion for a single constituent system, i.e.

$$\frac{d\hat{\rho}}{dt} = -\frac{i}{\hbar} [\hat{H}, \hat{\rho}] - \frac{1}{\tau} \hat{D} \quad (1)$$

and by the energy eigenvalue problem written as

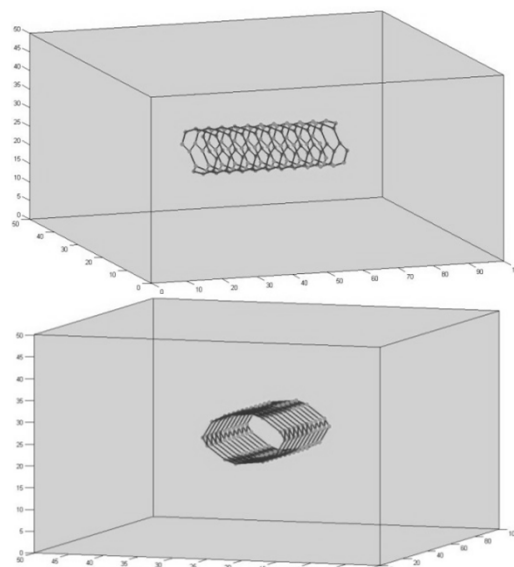


Figure 1. Schematic of the closed, isolated system containing the carbon nanotube and the hydrogen gas.

$$\hat{H}u_i(\vec{x}_1, \vec{x}_2, \dots, \vec{x}_n) = E_i u_i(\vec{x}_1, \vec{x}_2, \dots, \vec{x}_n) \quad (2)$$

for  $i = 1, 2, \dots, L$ . Note that in equation (1), the brackets are Poisson brackets.

Equation (1) implies both the first and the second laws of thermodynamics (von Spakovsky, 2008) and describes the non-linear dynamics of the system undergoing, for example, an irreversible process in the energy-entropy plane, something *not* possible with the linear dynamics of conventional and statistical quantum mechanics. In this equation,  $\hat{\rho}$  is a state operator<sup>1</sup>,  $\hat{H}$  the Hamiltonian operator,  $\tau$  a scalar time constant or functional<sup>2</sup>, and  $-\hat{D}/\tau$  the so-called dissipation term, which is a function of  $\hat{\rho}$ ,  $\ln \hat{\rho}$ , and  $\hat{H}$ , and which captures the nonlinear dynamics by pulling the state operator in the direction of the projection of the gradient of the entropy functional  $S = -kTr(\hat{\rho} \ln \hat{\rho})$  onto the hyper-plane of the constant energy (expectation value) of the system  $E = Tr(\hat{\rho} \hat{H})$ .

As to the second governing equation or system of equations, equation (2),  $E_i$  and  $u_i$  are the system-level energy eigenvalues and eigenfunctions, the  $\vec{x}_k$  are the 3D particle position vectors, and  $L$  is the number of system-level energy eigenvalues. It is assumed for the sake of simplicity that there are only translational modes of energy storage and degeneracies although the authors are currently in the process of incorporating internal modes of storage due to vibration and rotation that include rotational and spin

<sup>1</sup> The state operator is a linear, self-adjoint, non-negative definite, unit-trace operator (i.e. an operator whose diagonal elements sum to one) on Hilbert space  $\mathcal{H}$ . At a given instance of time, it is a representation of the state of a system which catalogues how the energy of the system is distributed amongst the various energy eigenlevels of the system. This state operator is based on a *homogeneous* ensemble of identical systems, identically prepared, i.e. on an *unambiguous* preparation (Hatsopoulos and Gyftopoulos, 1976d). This contrasts with the state operator of statistical quantum mechanics, which is based on a *heterogeneous* ensemble of identical systems, not identically prepared, i.e. on an *ambiguous* preparation. The former leads to a true unification of thermodynamics and mechanics while the latter results merely in a bridging with a built-in violation of the second law of thermodynamics, i.e. a perpetual motion machine of the second kind.

<sup>2</sup> Note, that a lower bound for  $\tau$  and, thus, an upper bound on  $\hat{D}$  has been established from the time-energy Heisenberg uncertainty relation (Beretta, 2001).

degeneracies in the quantum mechanical description. For the purposes of this paper, however, the Hamiltonian operator, which is written as

$$\hat{H} = \sum_{k=1}^n \left( \frac{-\hbar}{2m} \nabla_k^2 + V_k(\vec{x}_1, \vec{x}_2, \dots, \vec{x}_n) \right) \quad (3)$$

only represents the kinetic and potential energies of the translational motions of the H<sub>2</sub> particles in the tank and the intermolecular interactions between H<sub>2</sub> particles and between the H<sub>2</sub> and C particles of the carbon nanotube.

### 2.2.1 The energy eigenvalue problem

As the number of particles in the system increases, the eigenvalue problem, which represents a multi-body problem, very quickly becomes computationally difficult if not impossible to solve. This can be circumvented by assuming a set of 2-body problems (Hatsopoulos and Gyftopoulos, 1979) which define the motions and interactions between pairs of H<sub>2</sub> molecules (an H<sub>2</sub> and its nearest neighbour) and between each of these two H<sub>2</sub> molecules and the C atoms located on the nanotube<sup>3</sup>. For the H<sub>2</sub>-C motions and interactions, the 2-body problem is given by

$$\hat{H}_k u_j(\vec{x}_k) = \varepsilon_{k_j} u_j(\vec{x}_k), \quad j=1,2,\dots,M \quad (4)$$

for  $k = 1,2$  (i.e., the 1<sup>st</sup> and 2<sup>nd</sup> H<sub>2</sub>) and the translational Hamiltonian operator by

$$\hat{H}_k = \frac{-\hbar}{2m} \nabla_k^2 + \sum_l V_l(\vec{x}_k) \quad (5)$$

where the summation includes all of the H<sub>2</sub>-C interactions and the potential functions  $V_l(\vec{x}_k)$  are expressed by a 6-12 Lennard-Jones potentials, i.e.,

$$V(\vec{x}_k) = 4\xi \left[ \left( \frac{\sigma}{r(\vec{x}_k)} \right)^{12} - \left( \frac{\sigma}{r(\vec{x}_k)} \right)^6 \right] \quad (6)$$

Both  $\xi$  and  $\sigma$  are fitting parameters specific to a particular interaction (see Table 1), and  $r$  is the distance between molecules/atoms.

Table 1: Fitting parameters for the L-J potential.

Interaction	$\xi$ [J]	$\sigma$ [nm]
H <sub>2</sub> -H <sub>2</sub>	$5.24 \times 10^{-22}$	0.2915
H <sub>2</sub> -C	$4.502 \times 10^{-22}$	0.3137

Now, each  $\varepsilon_{k_j}$ , which appears in equation (4), is a paired particle or so-called primitive-level energy eigenvalue related to the system-level energy eigenvalues  $E_{k_i}$  by

$$E_{k_i} = \sum_{j=1}^M v_{ij} \varepsilon_{k_j} \quad (7)$$

The  $v_{ij}$  occupation coefficients are the number of paired H<sub>2</sub>-H<sub>2</sub> molecules for a given primitive energy eigenlevel  $j$  that occupy a given system energy eigenlevel  $i$ . When only a single pair of H<sub>2</sub> molecules are present (i.e., for  $N=1$ ), all

the  $v_{ij}$  are one. For a closed, non-reacting system and  $N \geq 2$ ,  $L$  is

$$L = (N + M - 1)! / (N!(M - 1)!) \quad (8)$$

where  $M$  is the total number of primitive energy eigenlevels. In general,  $M$  is infinite for the translational Hamiltonian operator since this operator is unbounded. However, for obvious computational reasons,  $M$  is assumed finite, an assumption which under certain conditions is justified as described below in the discussions surrounding Figure 15.

For the paired H<sub>2</sub>-H<sub>2</sub> motions, the 2-body problem expressed as

$$\hat{H}_{1,2} u_j(\vec{x}_1, \vec{x}_2) = \varepsilon_{1,2_j} u_j(\vec{x}_1, \vec{x}_2), \quad j=1,\dots,M \quad (9)$$

and the Hamiltonian as

$$\hat{H}_{1,2} = \sum_{k=1}^2 \frac{-\hbar}{2m} \nabla_k^2 + V(\vec{x}_1, \vec{x}_2) \quad (10)$$

is equivalently decomposed into a reduced mass ( $rm$ ) and a center of mass ( $cm$ ) problem (e.g., Shankar, 1994) such that

$$\hat{H}_k u_j(\vec{x}_k) = \varepsilon_{k_j} u_j(\vec{x}_k), \quad j=1,2,\dots,M \quad (11)$$

Here  $k = rm, cm$  so that the Hamiltonian for both the reduced mass and center of mass problems is written as

$$\hat{H}_k = \frac{-\hbar}{2m_k} \nabla_k^2 + V(\vec{x}_k) \quad (12)$$

The respective masses and coordinates for each of these problems are given by

$$m_{rm} = \frac{m_1 m_2}{m_1 + m_2} \quad (13)$$

$$m_{cm} = m_1 + m_2 \quad (14)$$

$$\vec{x}_{rm} = \vec{x}_2 - \vec{x}_1 \quad (15)$$

$$\text{and } \vec{x}_{cm} = \frac{m_1 \vec{x}_1 + m_2 \vec{x}_2}{m_1 + m_2} \quad (16)$$

Note that the potential function  $V(\vec{x}_k)$  in equation (12) is either zero for the center of mass problem or expressed by the 6-12 Lennard-Jones potential in equation (6) for the reduced mass problem.

Once the solutions to the set of 2-body problems listed above have been determined, they are assembled into a set of primitive-level energy eigenfunctions and eigenvalues so that for  $j=1,\dots,M$

$$u_j(\vec{x}_1, \vec{x}_2, \vec{x}_{rm}, \vec{x}_{cm}) = \prod_{k=1,2,rm,cm} u_j(\vec{x}_k) \quad (17)$$

$$\text{and } \varepsilon_j = \sum_{k=1,2,rm,cm} \varepsilon_{k_j} \quad (18)$$

Note that equations (17) and (18) imply a certain ‘‘coarse graining’’ of the available energy eigenstates, which for the results presented here has been done in a rather ad hoc fashion based on the primary quantum numbers. A more systematic approach has since been developed by the authors and will be reported in the near future. Also note that when  $N \geq 2$  (i.e., there are 2 or more H<sub>2</sub>-H<sub>2</sub> pairs), a

<sup>3</sup> Note that a similar approach is used when deriving stable equilibrium property relations from quantum thermodynamics such as, for example, the virial equation of state.

set of system-level energy eigenfunctions and eigenvalues must be determined based on the primitive-level ones. This is done by first determining the  $v_{ij}$  coefficients in equation (19) via a combinatorial problem which fills an  $L \times M$  matrix of possible occupation energies from which the system-level energy eigenvalues,  $E_i$ , are found using

$$E_i = \sum_{j=1}^M v_{ij} \varepsilon_j \quad (19)$$

To find the system-level  $u_i$ , the primitive-level  $u_j$  are first projected from the decomposed space represented by  $(\vec{x}_1, \vec{x}_2, \vec{x}_{rm}, \vec{x}_{cm})$  back onto 3D space represented by  $(\vec{x} = \{x, y, z\})$  and then combined using

$$u_i(\vec{x}) = \prod_{j=1 \text{ and } u_j \neq 0}^M (u_j(\vec{x}))^{v_{ij}} \quad (20)$$

This last result, equation (20), is a set of spatially dependent eigenfunctions, which are independent of time since the Hamiltonian operator and the boundary conditions (i.e., the tank and location of the carbon atoms) are fixed.

### 2.2.2 The equation of motion

Of course, to complete the thermodynamic description of the process which the system of Figure 1 undergoes, one must combine the solutions of the energy eigenvalue problem just described with that of the equation of motion, equation (1). In addition, since this is an initial-value problem, an initial condition for the system, i.e., an initial non-equilibrium state represented by an initial state operator or matrix  $\hat{\rho}$ , must be determined. This can be done randomly or as is done here using the procedure outlined in Beretta (2006b) and Smith and von Spakovsky (2007), which finds a set of partially canonical equilibrium states and then perturbs them to find a set of initial non-equilibrium states.

For the system of Figure 1 and the irreversible process of hydrogen storage considered here, equation (1) reduces to

$$\frac{d\hat{\rho}}{dt} = -\frac{1}{\tau} \hat{D} \quad (21)$$

for the case when  $\hat{\rho}$  is diagonal in the  $\hat{H}$  representation<sup>4</sup> since in this case  $\hat{H}$  commutes with  $\hat{\rho}$ . Equation (21) written out in terms of the eigenvalues  $\rho_i$  (probabilities) of  $\hat{\rho}$  (for this particular case, the diagonal elements of  $\hat{\rho}$ ) yields (for  $i=1, \dots, L$ )

$$\frac{d\rho_i}{dt} = \frac{1}{\tau} \frac{\begin{vmatrix} \rho_i \ln \rho_i & \rho_i & E_i \rho_i \\ \sum \rho_i \ln \rho_i & 1 & \sum E_i \rho_i \\ \sum E_i \rho_i \ln \rho_i & \sum E_i \rho_i & \sum E_i^2 \rho_i \end{vmatrix}}{\begin{vmatrix} 1 & \sum E_i \rho_i \\ \sum E_i \rho_i & \sum E_i^2 \rho_i \end{vmatrix}} \quad (22)$$

<sup>4</sup> Indeed, according to the Beretta equation, an initial  $\hat{\rho}$ , which is diagonal in the  $\hat{H}$  representation, remains diagonal at all times  $t$ . We consider this special class of diagonal initial states for simplicity and because in this case the eigenvalue  $\rho_i$  of  $\hat{\rho}$  is readily interpreted as the probability of finding the system in the system-level energy eigenvalue  $E_i$ . Nonetheless, it should be emphasized that the equation yields well-defined evolutions for arbitrary non-equilibrium initial states  $\hat{\rho}$  not necessarily diagonal in the  $\hat{H}$  representation, i.e., when  $\hat{H}$  and  $\hat{\rho}$  do not commute.

The dissipation term in equations (21) or (22) moves the system's entropy in the local direction of "steepest entropy ascent" Beretta (2006b) at constant energy  $E = \sum_{i=1}^L \rho_i E_i$  and composition. This is expressed explicitly in terms of the time evolution of  $S = -k \sum_{i=1}^L \rho_i \ln \rho_i$  by the entropy balance written as

$$\frac{dS}{dt} = \frac{k}{\tau} \frac{\begin{vmatrix} \sum \rho_i (\ln \rho_i)^2 & \sum \rho_i \ln \rho_i & \sum E_i \rho_i \ln \rho_i \\ \sum \rho_i \ln \rho_i & 1 & \sum E_i \rho_i \\ \sum E_i \rho_i \ln \rho_i & \sum E_i \rho_i & \sum E_i^2 \rho_i \end{vmatrix}}{\begin{vmatrix} 1 & \sum E_i \rho_i \\ \sum E_i \rho_i & \sum E_i^2 \rho_i \end{vmatrix}} \quad (23)$$

where the entropy generation term to the right of the equals is always non-decreasing.

### 2.2.3 Evolution in time of the thermodynamic state and position

Finally, with all the eigenvalues  $\rho_i$  of the state operator  $\hat{\rho}$  known at each instant of time  $t$  and the translational eigenfunctions  $u_i$  as a function of space  $\vec{x}$ , the probability distribution function  $\Phi(\vec{x}, t)$  for the evolution in time and space of the state of the hydrogen particles is found from

$$\Phi(\vec{x}, t) = \sum_{i=1}^L \rho_i(t) |u_i(\vec{x})|^2 \quad (24)$$

The first moment of this distribution function, which is used in the results presented below, is the mass density expressed as a function of time by

$$\rho(t) = \frac{\iiint \Phi m_{H_2} n dV}{\iiint dV} \quad (25)$$

where  $m_{H_2}$  is the mass of a hydrogen molecule and  $n$  the number of these molecules in the system.

## 3. Numerical Approach

### 3.1 Numerical Approach for Solving the Energy Eigenvalue Problems for Translation

The governing equations represented by the eigenvalue problem for translation (equation (2)) are numerically solved by the finite-element method (FEM). A proper weak formulation is used in order to apply FEM to this problem, i.e.,

$$\int \nabla u \cdot \nabla v d\vec{x} + \int V(\vec{x}) u v d\vec{x} = \epsilon \int u v d\vec{x} \quad (26)$$

where  $v$  is called the test function and  $\epsilon$  is the eigenvalue considered. The solution  $u$  has been approximated by second order Lagrange polynomials  $\varphi_j$ , namely,

$$u(\vec{x}) = \sum_{j=1}^{N_h} u_j \varphi_j(\vec{x}) \quad (27)$$

From equations (26) and (27), the following generalized eigenvalue problem can be deduced:

$$\hat{K} \vec{u} = \epsilon \hat{M} \vec{u} \quad (28)$$

where  $\vec{u} = (u_j)$ ,  $\hat{K}$  is the stiffness matrix, and  $\hat{M}$  is the mass matrix, the elements of which are given by

$$K_{ij} = \int \nabla \varphi_i \cdot \nabla \varphi_j d\vec{x} + \int V(\vec{x}) \varphi_i \varphi_j d\vec{x} \quad (29)$$

$$M_{ij} = \int \varphi_i \varphi_j d\vec{x} \quad (30)$$

In the case of the center of mass (*cm*) problem, the potential is zero, i.e.,  $V(\vec{x})=0$ . In this latter case, the stiffness matrix is the following:

$$K_{cm,ij} = \int \nabla \varphi_i \cdot \nabla \varphi_j d\vec{x} \quad (31)$$

Matrices  $\hat{K}$  and  $\hat{M}$  are properly modified to match the boundary conditions. The generalized eigenvalue problem (equation (2)) is solved by the Arnoldi algorithm (Arnoldi, 1951; Quarteroni, Sacco, and Saleri, 2000) applied to a shifted and inverted matrix with restarts until the eigenvalues are found. Solutions are considered to be converged after the residuals are less than  $1.0 \times 10^{-6}$ . The adopted grid consists of an unstructured mesh of 149,000 elements to ensure a grid independent solution.

### 3.2 Numerical Approach for Solving the Beretta Equation of Motion

A system of 10,000 first order ordinary differential equations (ODEs) are generated from the Beretta equation of motion of equation (22) and used to determine the evolution in state of the system in Figure 1. This system of equations is solved numerically forward and backwards in time using a Runge-Kutta 4,5 (RKF45) method, starting from an arbitrarily chosen dimensionless time of  $t^* = -2$ . This Runge-Kutta-Fehlberg method (Fehlberg, 1969, 1970; Hairer, Nørsett, and Wanner, 1993) uses a fourth order approach together with a fifth order one by employing all of the points of the former plus one additional calculation required by a Runge-Kutta 5 method. The RKF45 method is, thus, able to estimate and control the error in the solution and determine an appropriate step size automatically. This makes the method efficient for ordinary problems of automated numerical integration of ODEs.

### 4. Results

Figures 2 to 7 show the evolution in time of the probability distribution function (equation (24)) for the system of Figure 1 comprised of four hydrogen molecules ( $N=2$ ) and the 132 carbon atoms that make up the carbon nanotube. The two cases shown are distinguished by their beginning non-equilibrium states at  $t^*=-2$ . Note that Figures 2 to 7, which appear in grayscale here, were originally published in color in the ECOS09 proceedings. They can be found in color in the journal paper published on-line at [http://www.icatweb.org/j\\_content.htm](http://www.icatweb.org/j_content.htm). To distinguish the various regions in grayscale, note that the large dark background areas are regions of near zero probability density whereas the lighter color areas are regions of medium probability density. The small dark elliptical shaped areas completely contained within the lighter areas are regions with the highest probability densities. Thus, for case 1, at the initial state, one can see in Figure 2 that the highest values of the probability distribution function and, therefore, the highest densities of hydrogen occur at two places in the tank, one to the left of the carbon nanotube's center about halfway between the tube and the tank wall and the other to the right of this center, also situated about halfway between the tube and the opposite tank wall. There is very little if any hydrogen inside the carbon nanotube. Figure 3, on the other hand, shows that for case 2, the initial non-equilibrium state has the highest probability densities of hydrogen occurring in only one place in the tank, i.e., up and to the left of the carbon nanotube's center about three quarters of the way between the tube and the tank wall.

Again, there is very little if any hydrogen inside the carbon nanotube.

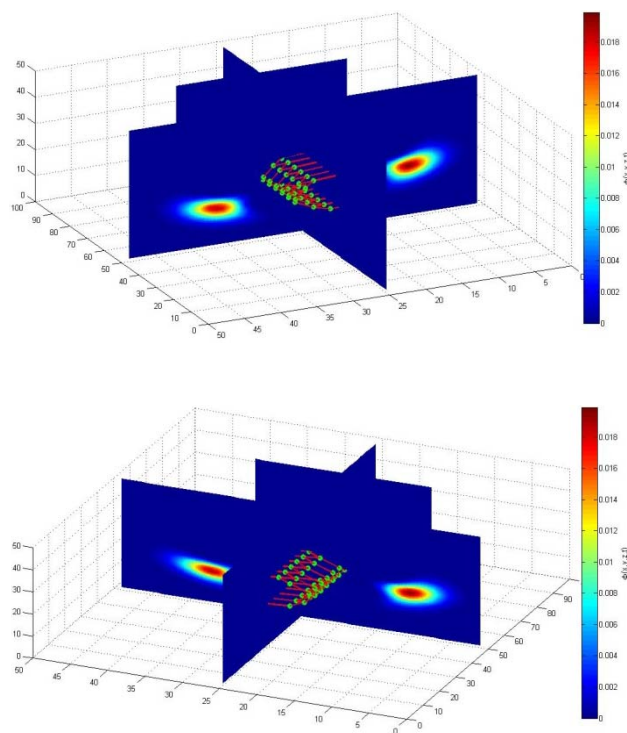


Figure 2. A plot for case 1 of the probability density (probability distribution function) of particle position as a function of position at  $t^*=-2$  with  $N=2$ ,  $M=143$ , and 10,000 system-level energy eigenlevels utilized.

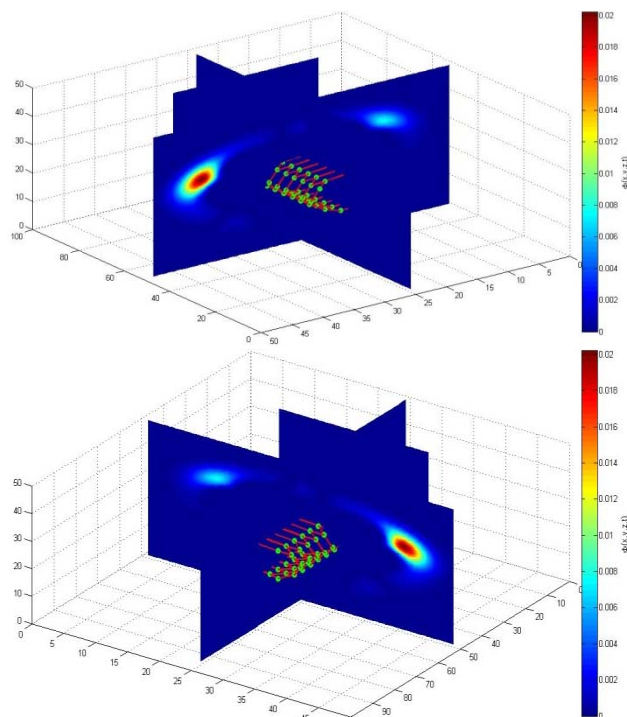


Figure 3. A plot for case 2 of the probability density (probability distribution function) of particle position as a function of position at  $t^*=-2$  with  $N=2$ ,  $M=143$ , and 10,000 system-level energy eigenlevels utilized.

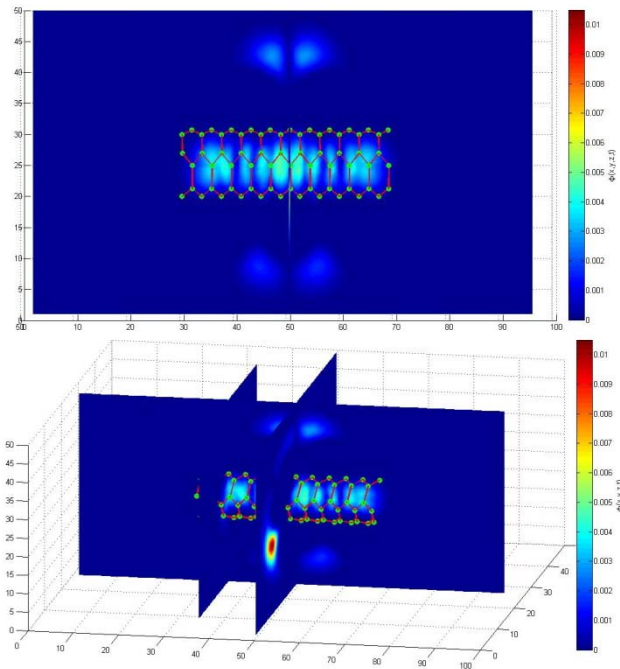


Figure 4. A plot for case 1 of the probability density (probability distribution function) of particle position as a function of position at  $t^*=-0.5$  with  $N=2$ ,  $M=143$ , and 10,000 system-level energy eigenlevels utilized.

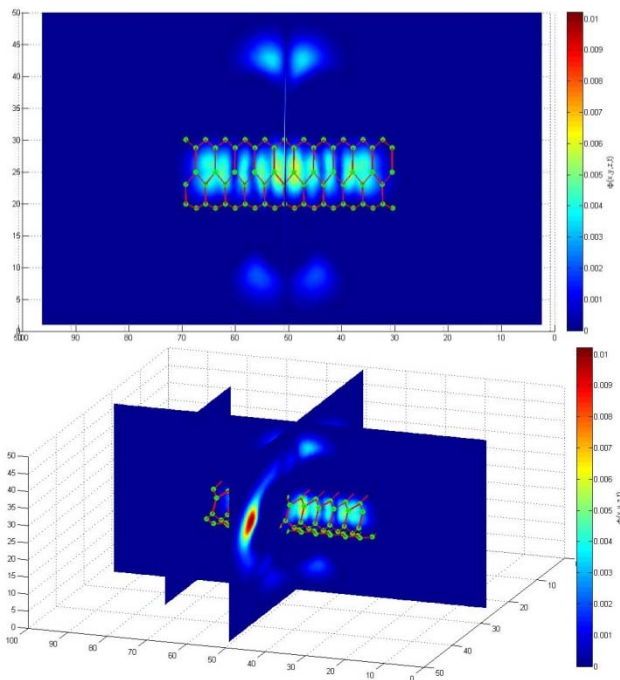


Figure 5. A plot for case 2 of the probability density (probability distribution function) of particle position as a function of position at  $t^*=-0.5$  with  $N=2$ ,  $M=143$ , and 10,000 system-level energy eigenlevels utilized.

From the initial states for cases 1 and 2, the state of the system evolves in time. Figures 4 and 5 show the states of the system at the intermediate time of  $t^*=-0.5$ . As can be seen in Figure 4, for case 1, the state of the system has evolved to the point that the value of the probability distribution function and, thus, the density of hydrogen has significantly increased in the interior of the carbon nanotube (i.e., from about zero to  $0.62 \times 10^{-4} \text{ kg/m}^3$ ). There is still a somewhat higher density to the left of the nanotube and another mirrored on the right of the tube (the

orientation of the second figure does not allow one see the latter but it is there) but both are diminished from the values seen in Figure 2 at the initial time.

As to case 2 and the state of the system at  $t^*=-0.5$ , Figure 5 shows that the value of the probability distribution function and, thus, the density of hydrogen has also significantly increased in the interior of the carbon nanotube and has, in fact, increased more than was the case for case 1 (i.e., from about zero to  $0.78 \times 10^{-4} \text{ kg/m}^3$ ). This higher concentration or density results in a much lower density to the left and the right of the nanotube than is still present at  $t^*=-0.5$  for case 1. Thus, for case 2, the system appears to be evolving more quickly towards stable equilibrium.

Figures 6 and 7 show the final state of the system at stable equilibrium for cases 1 and 2. As should be evident from the figures, the states of the system depicted are identical as would be expected since for a given value of the system expectation energy and for fixed composition and parameters (e.g., total volume), there is one and only one stable equilibrium state, i.e., it is unique (Hatsopoulos and Keenan, 1965; Hatsopoulos and Gyftopoulos, 1976a; Gyftopoulos and Beretta, 1991, 2005). This is in effect a statement of the Second Law of thermodynamics, which was initially proposed by Hatsopoulos and Keenan (1965). Furthermore, as is evident from these figures, the highest values of the probability distribution function and, thus, the hydrogen densities occur in the middle part of the tube and very little of the hydrogen is found any longer outside of the carbon nanotube. In fact, the hydrogen density inside the tube has more than doubled to  $2.0 \times 10^{-4} \text{ kg/m}^3$  from its previous value at  $t^*=-0.5$ . This can be seen more clearly in Figure 8, which shows the evolution of the hydrogen mass density as a function of time. Furthermore, the greater densities observed here in the interior of the tube at stable equilibrium are consistent with what has been observed both in a limited number of experiments and in, for example, the molecular dynamic (MD) simulations published in the literature (Banerjee and Puri, 2008). Note also that the temperature at stable equilibrium is about  $16.7 \text{ }^\circ\text{K}$  which means that the hydrogen quantum molecular model used here although incomplete is nonetheless consistent with a gaseous state for the hydrogen<sup>5</sup> since hydrogen has a triple point temperature of  $14 \text{ }^\circ\text{K}$  at 0.07 atm.

Now, in order to assess the irreversibilities which occurred during the two thermodynamic processes depicted in the previous figures, one can examine the rate of entropy generation shown in Figures 9a (case 1) and 9b (case 2) as well as the change in the entropy due to irreversibilities shown in Figures 10a (case 1) and 10b (case 2). The vast majority of the entropy creation and, thus, the increase in the entropy of the system occurs in a time interval of  $t^*=-2$  to  $t^*=-0$ . This corresponds with the largest number of energy eigenlevels coming into play, taking up a share of the overall system's energy and becoming occupied as the

<sup>5</sup> Obviously, the very simple quantum molecular model used in this paper is inadequate for describing all phases nor does it take into consideration the symmetric and anti-symmetric spin characteristics which result in the ortho- and para- forms of hydrogen, the latter being the predominant form of hydrogen at stable equilibrium. As mentioned earlier, a refinement of the quantum molecular model is currently underway and results for this updated model will be published in the near future.

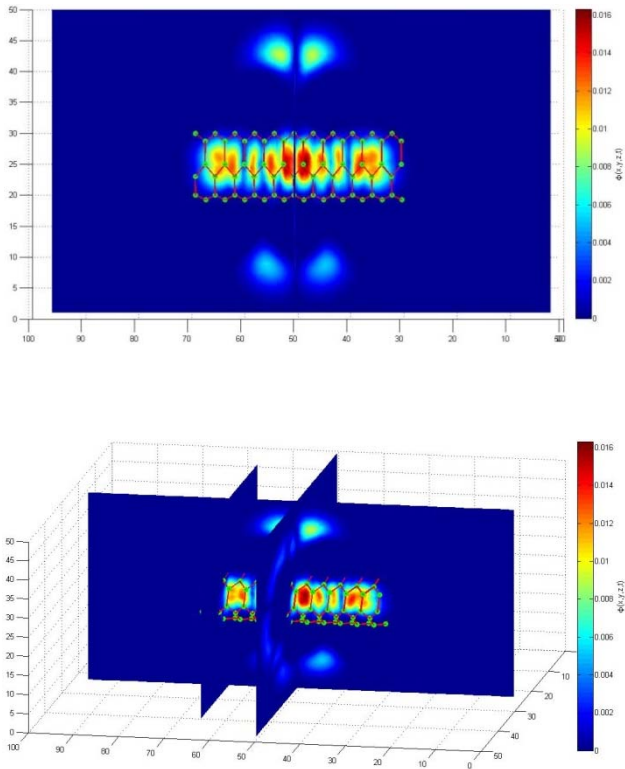


Figure 6. A plot for case 1 of the probability density (probability distribution function) of particle position as a function of position at  $t^*=5$  with  $N=2$ ,  $M=143$ , and 10,000 system-level energy eigenlevels utilized.

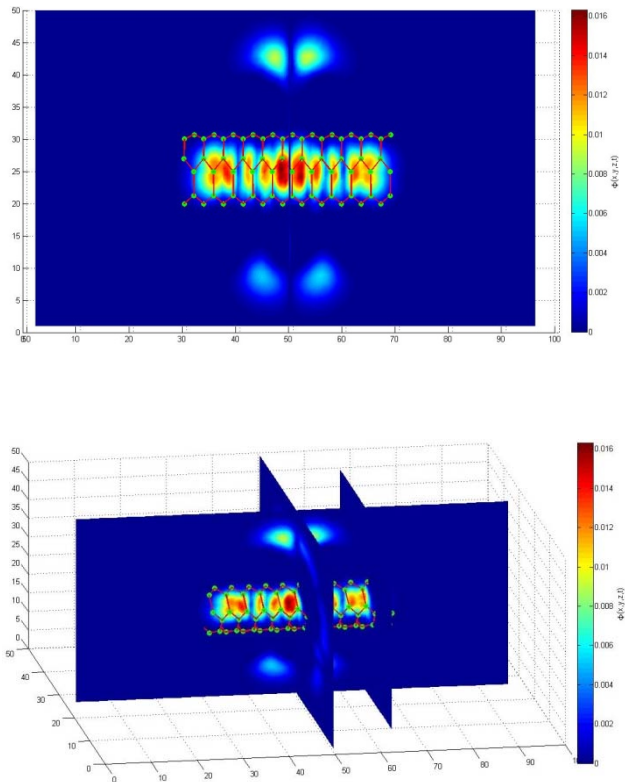


Figure 7. A plot for case 2 of the probability density (probability distribution function) of particle position as a function of position at  $t^*=5$  with  $N=2$ ,  $M=143$ , and 10,000 system-level energy eigenlevels utilized.

state of the system moves towards the stable equilibrium canonical distribution (see Figures 11 and 12). The total entropy generation for case 1 is computed to be  $7.164 \times 10^{-23}$  J/K and is smaller than that which occurs for case 2, which is found to be  $8.687 \times 10^{-23}$  J/K, a 21.2% increase over the first process. One of the implications of this is that if one could choose the initial state (or more importantly the final state if the process were reversed and one were discharging instead of charging the tank) intelligently one could control the thermodynamic path that the system followed and as a result reduce the losses incurred during the process.

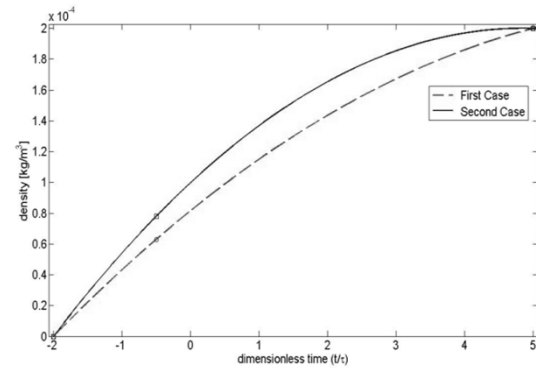
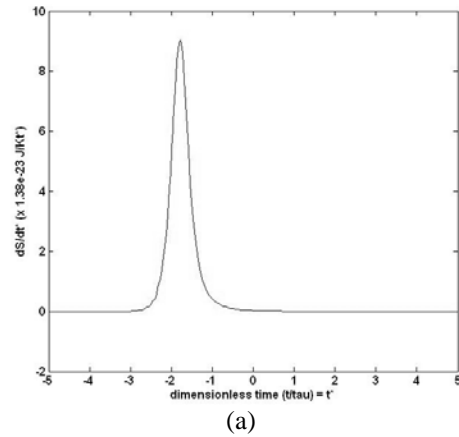
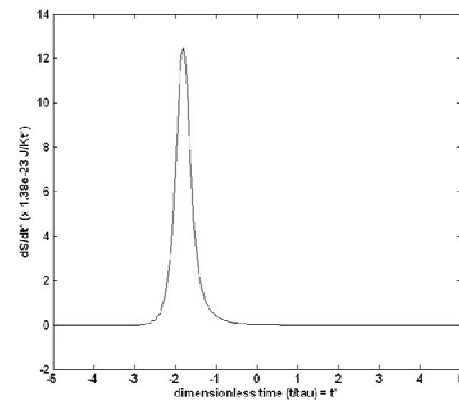


Figure 8. Plot of the mass density of hydrogen stored inside the carbon nanotube as a function of time.

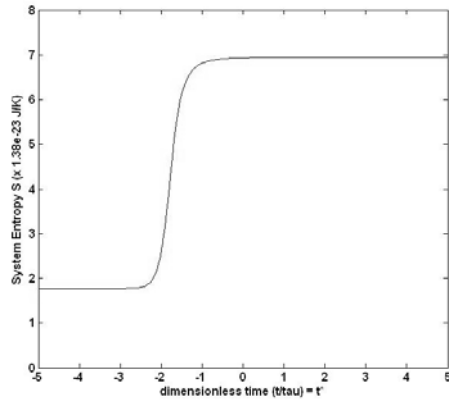


(a)

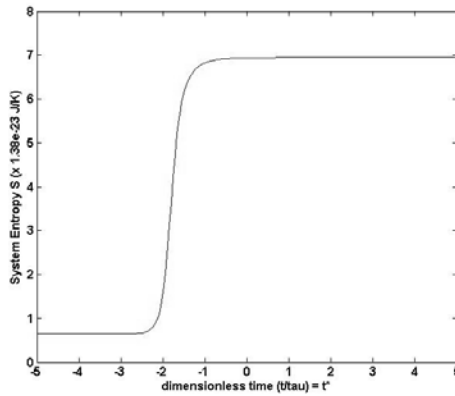


(b)

Figure 9. Time evolution of the entropy generation rate for cases 1 ((a)) and 2 ((b)) with  $N=2$ ,  $M=143$ , and 10,000 system energy eigenlevels utilized.

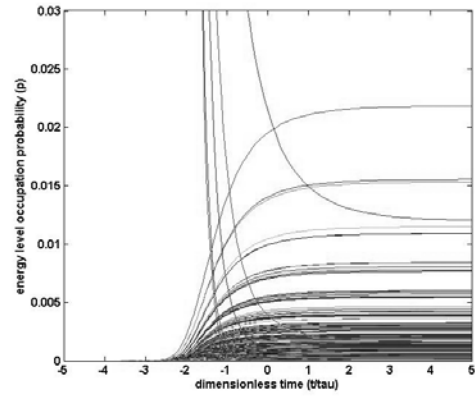


(a)

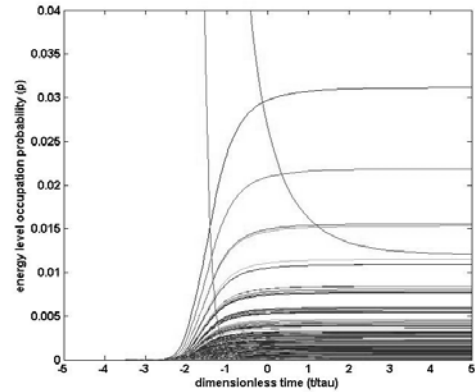


(b)

Figure 10. Time evolution of the entropy for cases 1 ((a)) and 2 ((b)) with  $N=2$ ,  $M=143$ , and 10,000 system energy eigenlevels utilized.

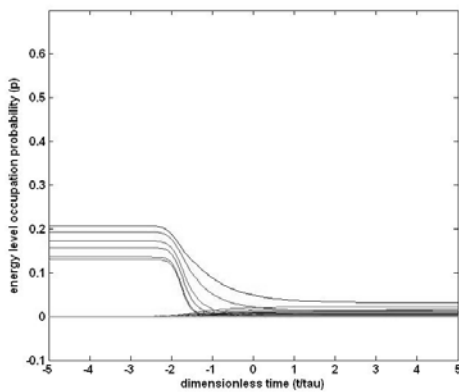


(a)

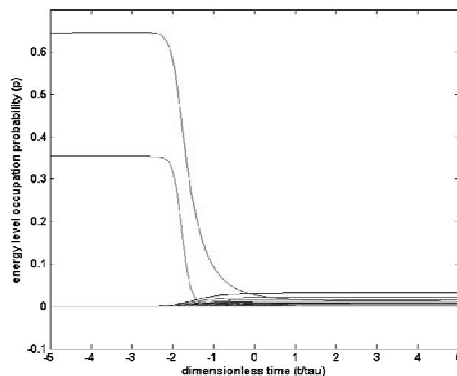


(b)

Figure 12. A zoomed-in plot of the time evolution of the probabilities of the state operator for cases 1 ((a)) and 2 ((b)) with  $N=2$ ,  $M=143$ , and 10,000 system-level energy eigenlevels utilized.



(a)



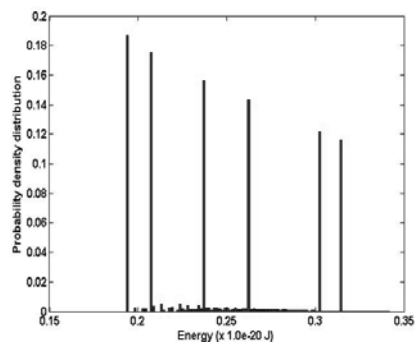
(b)

Figure 11. Time evolution of the probabilities of the state operator for cases 1 ((a)) and 2 ((b)) with  $N=2$ ,  $M=143$ , and 10,000 system-level energy eigenlevels utilized.

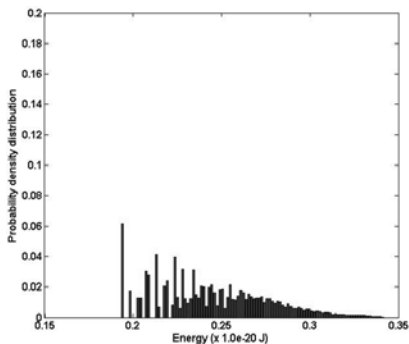
As already mentioned above, Figures 11 and 12 show the occupation histories of the energy eigenlevels for cases 1 and 2, i.e., they show the evolution of the thermodynamic state operator in time. As can be seen in Figures 11a and 11b, not all of the system-level energy eigenlevels are occupied at the early times and only gradually become occupied beginning at about  $t^*=-2.5$ , increasing their occupations until stable equilibrium is reached. This can be seen more clearly in the zoomed-in shot of Figures 12a and 12b. Figure 12b (case 2) in particular shows that at the earliest times (those approaching the primordial state at  $t^*=-5$ , i.e., the so-called “ancestral” state from which all succeeding states of the system originate), only two energy eigenlevels are occupied. This changes dramatically at about  $t^*=-2.5$  when many more come on-line.

Now in order to view the evolution in state of the system in Figure 1 in another more traditional light, the probability density distribution of energies is calculated for the non-equilibrium states through which the system passes as well as for the stable equilibrium state at which the system arrives. The results for the latter state and for two of the non-equilibrium states are shown in Figures 13 (case 1) to 14 (case 2). As can be seen in these figures, there is an evolution from a non-Maxwellian type of distribution at  $t^*=-2$  and at  $t^*=-0.5$  to a Maxwellian type of distribution at stable equilibrium. This is what one would expect but what is significant here is that one does not have to guess at the distributions since they fall directly out of the

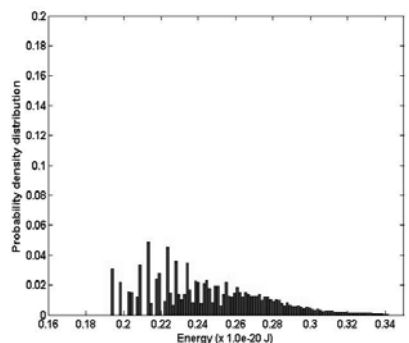
physics/thermodynamics of the problem captured by both the Beretta equation of motion and the energy eigenvalue problem associated with the behavior of the hydrogen molecules relative to each other and to the carbon atoms in the tank.



(a)



(b)

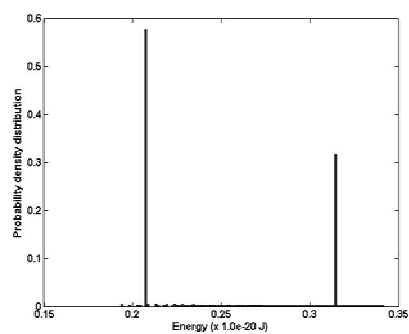


(c)

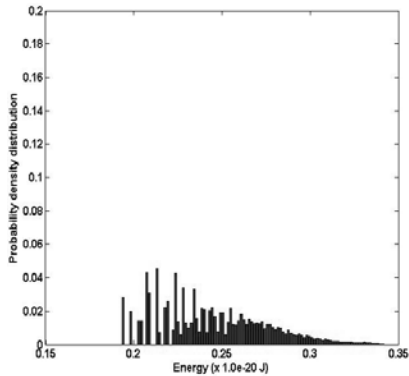
Figure 13. Plot of the probability density distribution of energies at  $t^*=-2$  ((a)),  $t^*=-0.5$  ((b)), and  $t^*=10$  ((c)) for case 1 with  $N=2$  and  $M$  varying between 143 and 10,000.

Finally, to determine the minimum number of finite energy eigenlevels required for modeling the evolution of state of the system to an acceptable level of accuracy, a plot of the system energy  $E$  (an expectation value) versus the system entropy  $S$  (also an expectation value) is made for different numbers of eigenlevels including the so-called limit curve of an infinite number of levels. The results are shown in Figure 15 along with the maximum thermodynamic temperature at which the accuracy for a

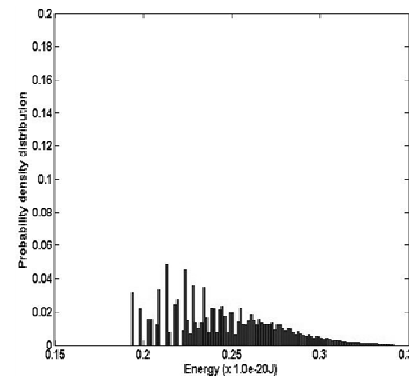
given number of finite energy eigenlevels begins to decrease. As can be seen, with 10,000 system energy eigenlevels utilized, the system can be modelled with good results for temperatures at stable equilibrium up to about 17 K. After that, the stable equilibrium curve for 10,000 levels begins to diverge significantly from the limit curve which is based on an infinite number of levels. To achieve higher temperatures, more system energy eigenlevels would have to be used. It should also be emphasized here that the thermodynamic temperature only has meaning at stable equilibrium and is not defined for non-equilibrium states. This, however, unlike in other approaches (e.g., MD), poses no problem for describing the thermodynamic evolution of state of the system since the equation of motion, the Beretta equation, does not require it.



(a)



(b)



(c)

Figure 14. Plot of the probability density distribution of energies at  $t^*=-2$  ((a)),  $t^*=-0.5$  ((b)), and  $t^*=10$  ((c)) for case 2 with  $N=2$  and  $M$  varying between 143 and 10,000.

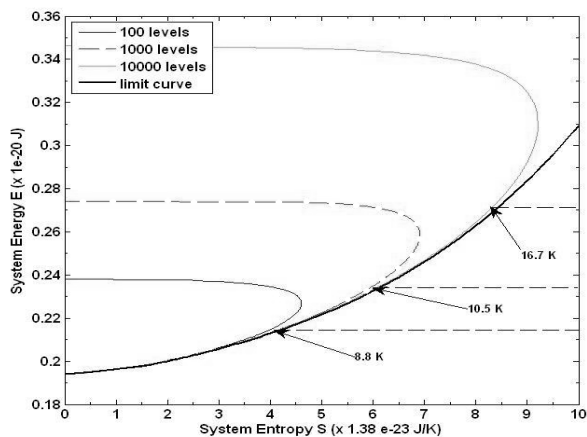


Figure 15. Expectation energy  $E$  versus the expectation entropy  $S$  for the 3D tank with  $N=2$  and  $M=143$  and the number of system-level energy eigenlevels varying between 100 and 10,000.

## 5. CONCLUSIONS

Quantum thermodynamics has been applied successfully in this paper to modeling in 3D the thermodynamic evolution in state and position of an atomistic or nanoscale system of hydrogen molecules contained in a tank at the center of which is a carbon nanotube. The thermodynamic description in time which results provides the exact path taken by the system in relaxing from some initial state far from stable equilibrium to a final state of stable equilibrium. The ability to do this at this level of description is unique to this paradigm of physics and thermodynamics since all other existing paradigms are in one way or another either equilibrium limited (i.e., require some assumption of local equilibrium or eschew this assumption for some maximization or minimization principle) or base their non-equilibrium description on a loss of information in the exogenous statistics, which inevitably leads to the conclusion that the entropy generation due to irreversibility emerges as a kind of *statistical illusion*.

Finally, the successful application of this new paradigm has been limited to date since any number of issues or problems remain to be resolved including how this paradigm can be applied to a much wider range of practical problems of interest (reacting systems, open systems, systems undergoing non-work interactions, high temperature systems, etc.). We are presently working on many of these issues.

## Nomenclature

$\hat{D}$	dissipation operator
$E$	expectation energy
$E_i$	system-level energy eigenvalue
$\hat{H}$	Hamiltonian operator
$\hbar$	modified Planck constant
$k$	Boltzmann's constant
$L$	number of system-level energy eigenlevels
$M$	number of primitive-level energy eigenlevels
$m$	mass
$N$	number of primitives
$n$	number of particles or molecules
$P(\epsilon)$	probability density distribution of energies
$S$	expectation entropy
$t$	time

$t^*$	dimensionless time equal to $t/\tau$
$u(\vec{x})$	energy eigenfunction
$V(\vec{x})$	interparticle potential function
$\vec{x}$	coordinate vector
$x$	x-coordinate
$y$	y-coordinate

## Greek

$\epsilon_j$	primitive-level energy eigenvalue
$\Phi(\vec{x}, t)$	probability distribution function of particle position in time
$V_{ij}$	occupation coefficients
$\hat{\rho}$	state operator
$\sigma$	fitting parameter for the L-J potential
$\tau$	scalar time constant or functional
$\xi$	fitting parameter for the L-J potential

## References

- Arnoldi, W. E., 1951, "The Principle of Minimized Iterations in the Solution of the Matrix Eigenvalue Problem," *Q. of Applied Mathematics*, 9, pp 17-29.
- Banerjee, S. and Puri, K., 2008, "Enhancement in hydrogen storage in carbon nanotubes under modified conditions," *Nanotechnology*, 19 (2008) 155702 (6pp).
- Beretta, G. P., 1981, "On the General Equation of Motion of Quantum Thermodynamics and the Distinction between Quantal and Nonquantal Uncertainties," Dr. Sc. thesis, MIT, Cambridge, MA.
- Beretta, G. P., 2001, <http://arxiv.org/abs/quant-ph/0112046>, Dec., pp 1-19.
- Beretta, G. P., 2005, "Nonlinear extensions of Schrodinger- von Neumann quantum dynamics: A set of necessary conditions for compatibility with thermodynamics," *Modern Physics Letters A*, 20(13), 977-984.
- Beretta, G. P., 2006a, "Nonlinear model dynamics for closed-system, constrained, maximal-entropy-generation relaxation by energy redistribution," *Physical Review E*, 73(2), 026113.1- 026113.11.
- Beretta, G. P., 2006b, "Steepest-entropy-ascent irreversible relaxation towards thermodynamic equilibrium: The dynamical ansatz that completes the Gyftopoulos-Hatsopoulos Unified Theory with a general quantal law of causal evolution," *Int. J. of Thermodynamics*, 9, 3, pp. 97-108.
- Beretta, G. P., 2007, "Well-behaved nonlinear evolution equation for steepest-entropy-ascent dissipative quantum dynamics," *International Journal of Quantum Information*, 5(1-2), 249-255.
- Beretta, G. P. "Nonlinear generalization of Schrödinger's equation uniting quantum mechanics and thermodynamics," *International Journal of Thermodynamics*, 11, 49-60, 2008.
- Beretta, G. P., Gyftopoulos, E. P., Park, J. L., and Hatsopoulos, G. N., 1984, *Il Nuovo Cimento*, 82 B, 2, pp. 169-191.
- Beretta, G. P., Gyftopoulos, E. P., and Park, J. L., 1985, "Quantum thermodynamics - a new equation of motion for

- a general quantum system," *Nuovo Cimento Della Societa Italiana Di Fisica B-General Physics Relativity Astronomy and Mathematical Physics and Methods*, 87(1), 77-97.
- Fehlberg, E., 1969, "Low-order classical Runge-Kutta formulas with step size control and their application to some heat transfer problems," NASA Technical Report 315.
- Fehlberg, E., 1970, "Klassische Runge-Kutta-Formeln vierter und niedrigerer Ordnung mit Schrittweiten-Kontrolle und ihre Anwendung auf Wärmeleitungsprobleme," *Computing (Arch. Elektron. Rechnen)*, vol. 6, pp. 61-71.
- Frey, J. T. and Doren, D. J., 2005, TubeGen 3.3 (web-interface, <http://turin.nss.udel.edu/research/tubegenonline.html>), University of Delaware, Newark, DE.
- Gheorghiu-Svirschevski, S., 2001, "Nonlinear quantum evolution with maximal entropy production," *Physics Review A*, 63, 022105.
- Gorini, V., Kossakowski, A., and Sudarshan, E. C. G., 1976, "Completely Positive Dynamical Semigroups of N-level Systems," *Journal of Mathematical Physics*, 17(5), pp. 821.
- Gyftopoulos, E. P. and Beretta, G. P., 1991, *Thermodynamics – Foundations and Applications*, Macmillan N. Y.
- Gyftopoulos, E. P. and Beretta, G. P., 2005, *Thermodynamics – Foundations and Applications*, Dover Pub., N. Y.
- Hairer, E., Nørsett, S., and Wanner, G., 1993, *Solving Ordinary Differential Equations I: Nonstiff Problems*, second edition, Springer-Verlag, Berlin.
- Harris, S., 1999, *An introduction to the Theory of the Boltzmann Equation*, Dover Publications, N.Y.
- Hatsopoulos, G. N. and Gyftopoulos, E. P., 1976a,b,c,d, "A Unified Quantum Theory of Mechanics and Thermodynamics – Part I: Postulates, Part IIa: Available Energy, Part IIb: Stable Equilibrium States, Part III: Irreducible Quantal Dispersions," *Foundations of Physics*, 6, 1, pp. 15-31, 2, pp. 127-141, 4, pp. 439-455, 5, pp. 561-570.
- Hatsopoulos, G. N. and Gyftopoulos, E. P., 1979, *Thermionic Energy Conversion – Vol. 2: Theory, Technology, and Application*, MIT Press, Cambridge, MA.
- Hatsopoulos, G. N. and Keenan, J. H., 1965, *Principles of General Thermodynamics*, Wiley, N. Y.
- Hill, T. L., 1956, *Statistical Mechanics: Principles and Selected Applications*, McGraw Hill Book Co., New York.
- Ingarden, R. S. and Kossakowski, A., 1975, "On the connection of non-equilibrium information thermodynamics with non-Hamiltonian quantum mechanics of open systems", *Ann. Phys. (N.Y.)*, 89, pp. 451.
- Kossakowski, A., 1972, "On Necessary and Sufficient Conditions for a Generator of a Quantum Dynamical Semigroup," *Bull. Acad. Sci. Math.* 20, pp. 1021, and "On Quantum Statistical Mechanics of Non-Hamiltonian Systems," *Rep. Math. Phys.*, 3, pp. 247.
- Liboff, R. L., 1979, *Introduction to the Theory of Kinetic Equations*, Krieger Publishing, N.Y.
- Lindblad, G., 1976, "On the Generators of Quantum Dynamical Semigroups," *Comm. Math. Phys.*, 48(2), pp. 119.
- Quarteroni, A., Sacco, R., Saleri, F., 2000, *Numerical Mathematics*, Springer, pp 215 - 218.
- Shankar, R., 1994, *Principles of Quantum Mechanics*, Springer Science & Business Media, Inc., N.Y.
- Smith, C. and von Spakovsky, M. R., 2007, "Time Evolution of Entropy in a System Comprised of a Boltzmann Type Gas: An Application of the Beretta Equation of Motion," *International Mechanical Engineering Congress and Exposition – IMECE'2007*, ASME Paper No. IMECE2007-42933, N.Y., N.Y., November.
- Smith, C. E., Verda, V., von Spakovsky, M. R., 2008, "Quantum Thermodynamics for the Modeling of Non-equilibrium Phenomena," *Efficiency, Costs, Optimization, Simulation and Environmental Aspects of Energy Systems (ECOS'08)*, keynote address, Cracow, Poland, ASME, June 24-27.
- Tien, C. L. and Lienhard, J. H., 1979, *Statistical Thermodynamics*, revised printing, Hemisphere Publishing Corp., Washington.
- von Spakovsky, M.R., 2008, "The Second Law: A Unified Approach to Thermodynamics Applicable to All Systems and All States," *Keenan Symposium: Meeting the Entropy Challenge*, MIT, American Institute of Physics (AIP), AIP Proceedings, Cambridge, MA, October 2007.
- von Spakovsky, M.R., Smith, C. E., Verda, V., 2008, "Quantum Thermodynamics for the Modeling of Hydrogen Storage on a Carbon Nanotube," *ASME International Mechanical Engineering Congress and Exposition – IMECE'2008*, ASME Paper No. IMECE2008-67424, N.Y., N.Y., Oct.-Nov.